Geophysical Research Letters
Supporting Information for

Drought legacy in sub-seasonal vegetation state and sensitivity to climate over the Northern Hemisphere

Minchao Wu[1,2]*, Stefano Manzoni[3,4], Giulia Vico[5], Ana Bastos[6], Franciska de Vries[7], Gabriele Messori[1,4,8,9]

[1] Department of Earth Sciences, Uppsala University, Uppsala, Sweden
[2] Department of Physical Geography and Ecosystem Science, Lund University, Lund, Sweden
[3] Department of Physical Geography, Stockholm University, Stockholm, Sweden
[4] Bolin Centre for Climate Research, Stockholm University, Stockholm, Sweden
[5] Department of Crop Production Ecology, Swedish University of Agricultural Sciences (SLU), Uppsala, Sweden
[6] Max-Planck Institute for Biogeochemistry, Department of Biogeochemical Integration, Hans-Knöll Str. 10, 07745 Jena, Germany
[7] Institute for Biodiversity and Ecosystem Dynamics, University of Amsterdam, 1090 GE Amsterdam, Netherlands
[8] Centre of Natural Hazards and Disaster Science (CNDS), Uppsala, Sweden
[9] Department of Meteorology, Stockholm University, Stockholm, Sweden
*Correspondence to: Minchao Wu, minchao.wu@geo.uu.se

Contents of this file

Supplementary Information

SI 1 Extended description of data

SI 1.1 Drought index SPEI

We quantified drought severity using the Standardised Precipitation-Evapotranspiration Index (SPEI, Vicente-Serrano et al., 2010). SPEI is a multiscalar drought index based on the climatic water balance represented as the difference between precipitation and potential evapotranspiration for a specific period. SPEI indicates water deficit if negative and surplus if positive. SPEI can be computed over different timescales representing the cumulative hydrological balance over previous numbers of months, typically between 1 and 48 months. Here, we choose SPEI at the time scale of one month (SPEI1) to identify extreme conditions associated with soil moisture deficits. SPEI at the time scales of three months (SPEI3) and six months (SPEI6) were also used to test the dependence of our results on SPEI time scales. The existing global SPEI dataset covers the period between January 1901 and December 2018 at 0.5-degree spatial resolution. To include the recent extreme events such as the period after 2018 Europe heatwave and droughts, we extend the dataset with the SPEI utility (Beguería, 2017) until the end of 2020, based on the latest CRU TS 4.05 dataset.

SI 1.2 Satellite-based vegetation index datasets

The MODIS enhanced vegetation index (EVI) captures changes in vegetation canopy greenness, which reflects leaf area, chlorophyll and canopy structure and is employed to represent vegetation state in our analysis. EVI improves sensitivity over high biomass vegetation relative to the Normalised Difference Vegetation Index (NDVI) by minimising noise from atmospheric influences and soil-brightness variations (Huete et al., 2002) and has been widely used to monitor mechanisms of vegetation response to droughts (Jiao et al., 2021a and references therein). The EVI dataset is produced at 16-day intervals at 0.05-degree resolution Climate Modeling Grid (CMG) cells, with a MODIS-specific compositing method to remove low-quality pixels.

SI 1.3 Datasets for growing conditions and other ancillary data

Three local growing conditions, i.e., 2m air temperature, downwards surface solar radiation, and root-zone soil moisture, were used to represent key vegetation limiting factors (temperature, light, and water) and to investigate changes in post-drought vegetation

sensitivity to climate. Monthly-mean 2m air temperature and downwards surface solar radiation at 0.25-degree horizontal resolution were derived from ERA5 reanalysis (Hersbach et al., 2020). Root-zone soil moisture was derived from the Global Land Evaporation Amsterdam Model (GLEAM, Martens et al., 2017), which employs a multi-layer water-balance algorithm considering the depth root zone being a function of the land-cover class. GLEAM soil moisture is at the same temporal and spatial resolutions as ERA5, and is suggested to in general outperform ERA5 reanalysis, in particular for the slow variability at monthly and longer timescales (Beck et al., 2021).

In addition, monthly frost day frequency at 0.5-degree horizontal resolution was used to locally define the growing season (see Wu et al., 2021, and Sect. 2.4 below). To investigate the influences of ecosystem type on vegetation response to droughts, we used the yearly 0.05-degree MODIS-based maps of the International Geosphere-Biosphere Programme (IGBP) land classification data set of MCD12C1 (Friedl et al., 2002) and grouped relevant spatial points for each land class (Fig. S3).

To gain further insight into the impacts of aridity on the identified legacy effects, we extended the land-cover classification by grouping data by aridity classes based on the Global Aridity Index (AI) provided by the Consultative Group on International Agricultural Research (CGIAR) Consortium for Spatial Information (CGIAR-CSI, https://cgiarcsi.community/data/global-aridity-and-pet-database/). AI is defined as the ratio of annual rainfall to annual potential evapotranspiration (Jiao et al., 2021b). Two aridity regions, humid (AI > 0.65) and arid (AI <= 0.2) (Fig. S14), were defined for the aridity-related analyses to separate the responses of vegetation adapted to either humid or dry environments (Fig. S15-16). Global irrigation maps from the ESA CCI Land Cover time-series v2.0.7 (Santoro et al., 2017) (1992-2015, at a 300m spatial resolution) are also used to verify the effectiveness of the employed filtering approach based on significant correlation coefficients.

SI 2 Figures

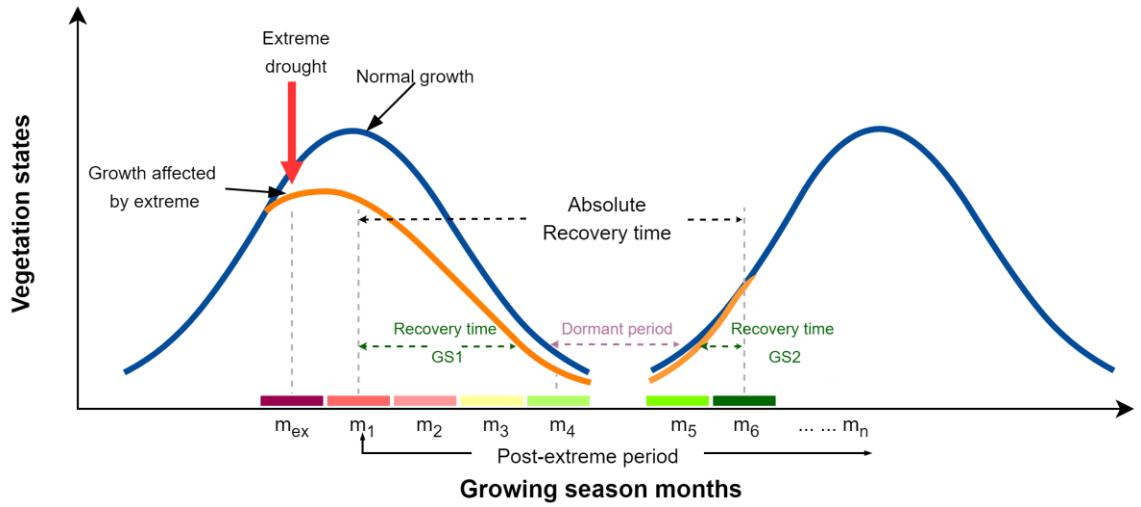

Fig. S1. Schematic diagram for identifying droughts and post-drought periods based on the location-specific definition of vegetation growing seasons. The recovery period starts from the month (m_1) after the extreme month (m_{ex}, i.e., the month in which a severe drought occurs), but does not include the dormant period between each growing season (purple dashed line). The recovery period ends when the post-drought vegetation state (orange solid line) returns to the normal vegetation state (dark blue solid line).

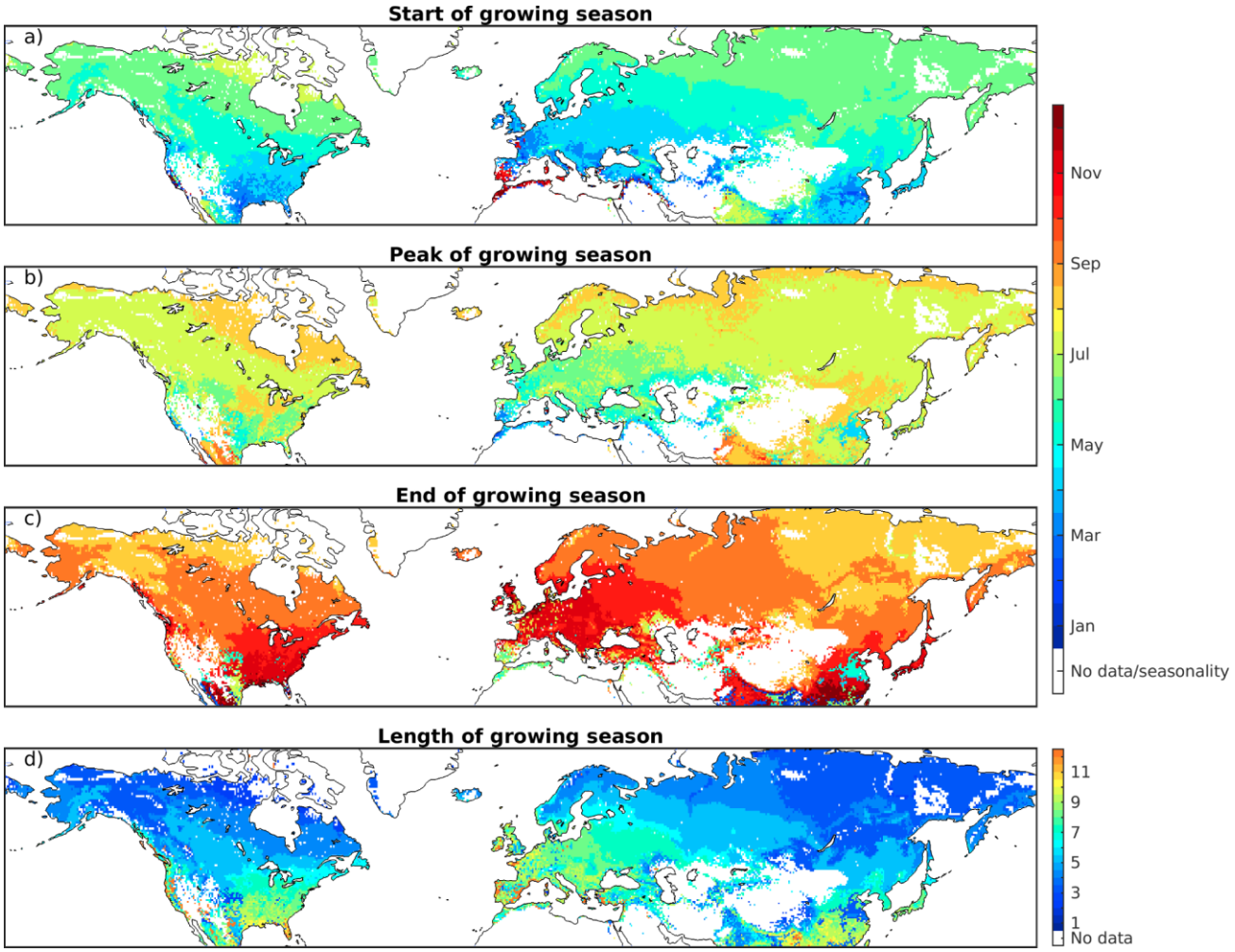

Fig. S2. Growing season parameters used to constrain the calculation of vegetation and climate variables in this study, which include: (a) start of growing season (SOS), (b) peak of growing season (POS), (c) end of growing season (EOS) and (d) length of growing season (LOS). Calculations are based on MODIS EVI data and CRU 4.1, see Methods for details.

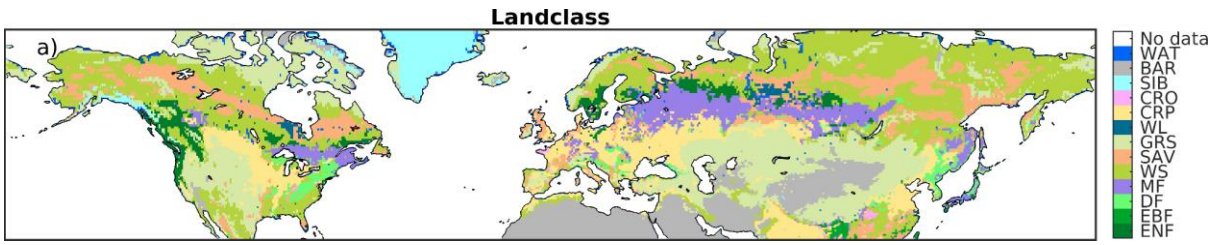

Fig. S3. Definition of land-cover classes based on IGBP land classes. The abbreviations in the colour bar refer to: ENF, evergreen needleleaf forests; EBF, evergreen broadleaf forests; DF, deciduous forests; MF, mixed forests; WS, closed shrubland, open shrubland and woody savannas; SAV, savannas (temperate); GRS, grasslands; WL, permanent wetland; CRP, croplands; CRO, croplands and natural vegetation mosaic; SIB, snow and ice; BAR, barren sparsely vegetation; WAT, water bodies.

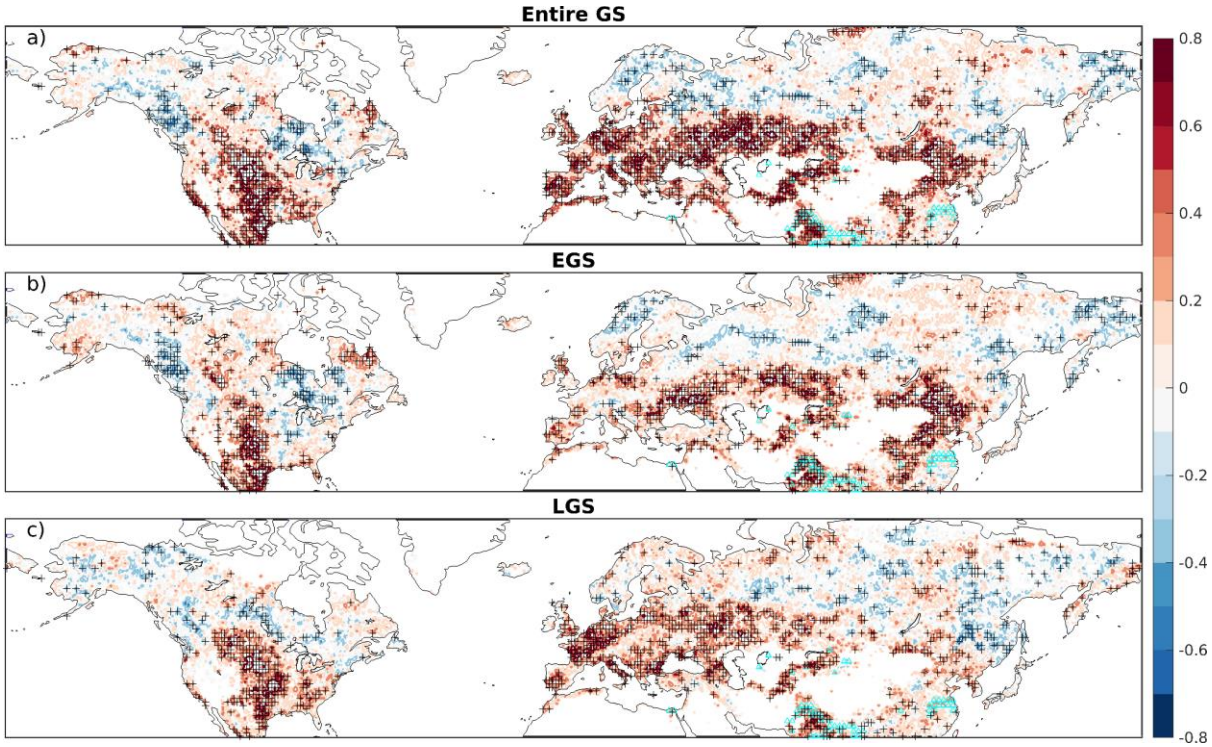

Fig. S4. Same as Fig. 1, but presenting gridpoints with significant r ($p < 0.05$; stippled with black "+") based on SPEI1 and gridpoints with intense irrigation (> 0.5 irrigation fraction of the gridpoint, in cyan).

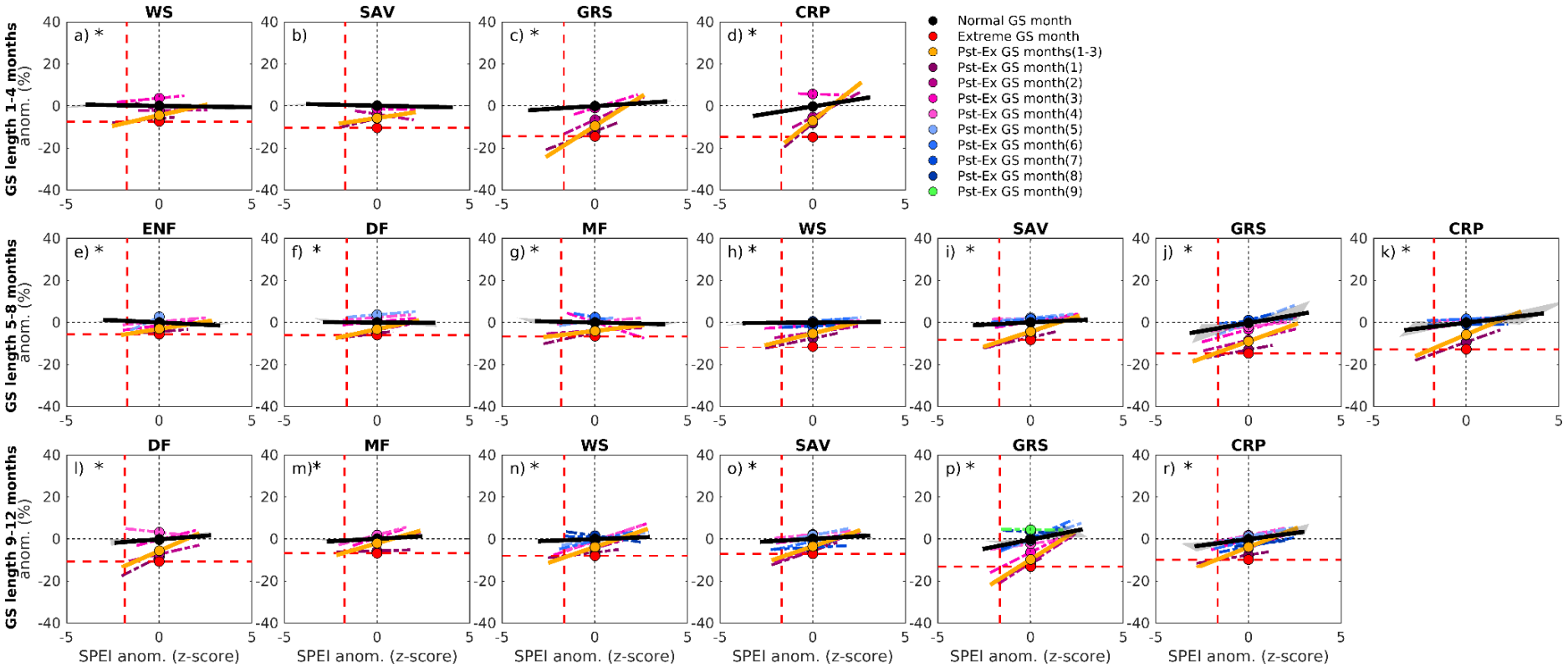

Fig. S5. Changes in vegetation state (EVI anomalies, y-axis, %) and sensitivities to SPEI1 for post-drought months relative to those in normal growing season (GS) months when severe droughts occur in early GS. Filled circles (excluding the red one) are the intercepts of linear regression models based on the EVI anomalies (y-axis, %) against the standardised SPEI1 anomalies (x-axis, z-score), indicating vegetation states for neutral growing conditions (i.e., α). Dashed lines excluding the red one are the slope of regressions for each GS month, indicating vegetation sensitivity (i.e., β). Red horizontal and vertical dashed lines indicate the average anomalies of EVI and SPEI1 when severe droughts occur. The red filled circle is used to compare the vegetation states for the normal and post-drought periods. Grey shading along the black solid line indicates the spread of sensitivities for different GS months during the normal period. Solid orange lines are slopes of the first three post-drought months. Stars in the top left corner indicate a significant difference between the black and orange solid lines.

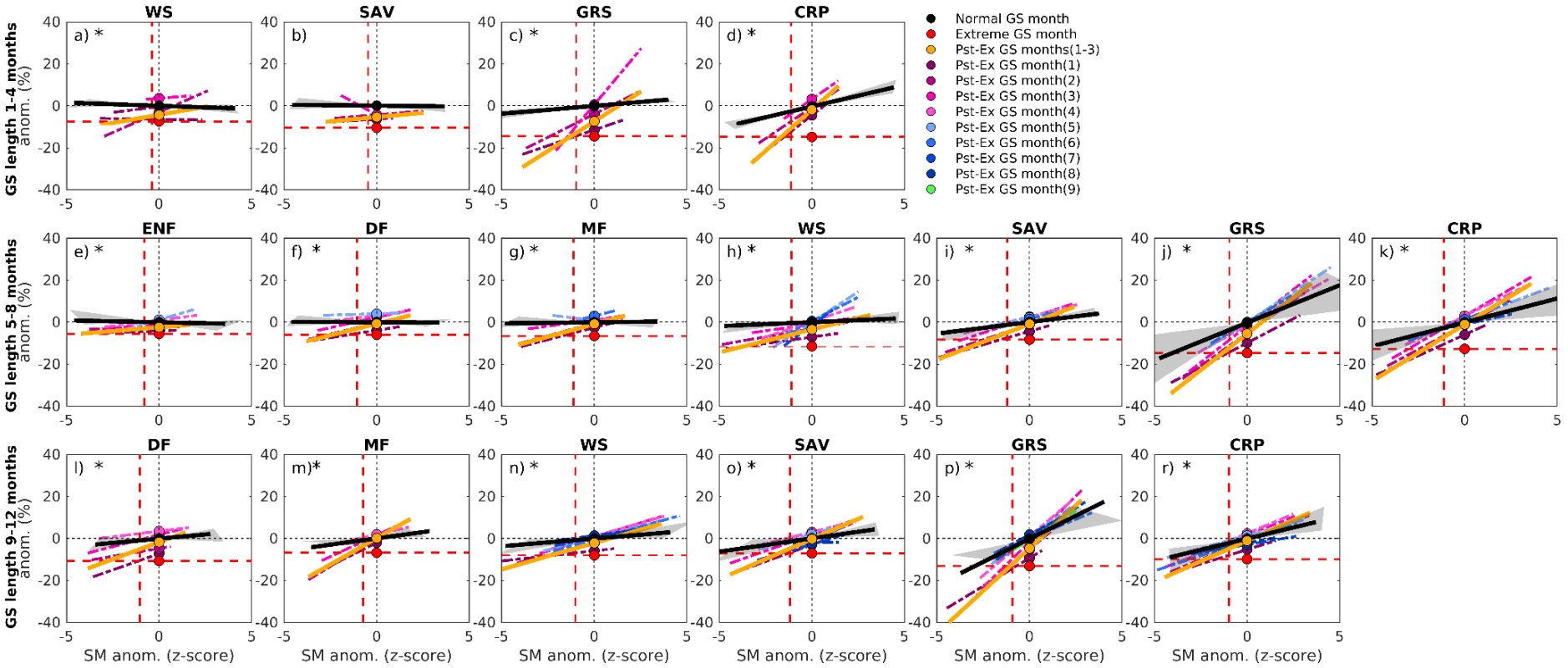

Fig. S6. Same as Fig. S5, but for EVI anomalies (y-axis, %) against the standardised soil moisture (SM) anomalies (x-axis, z-score).

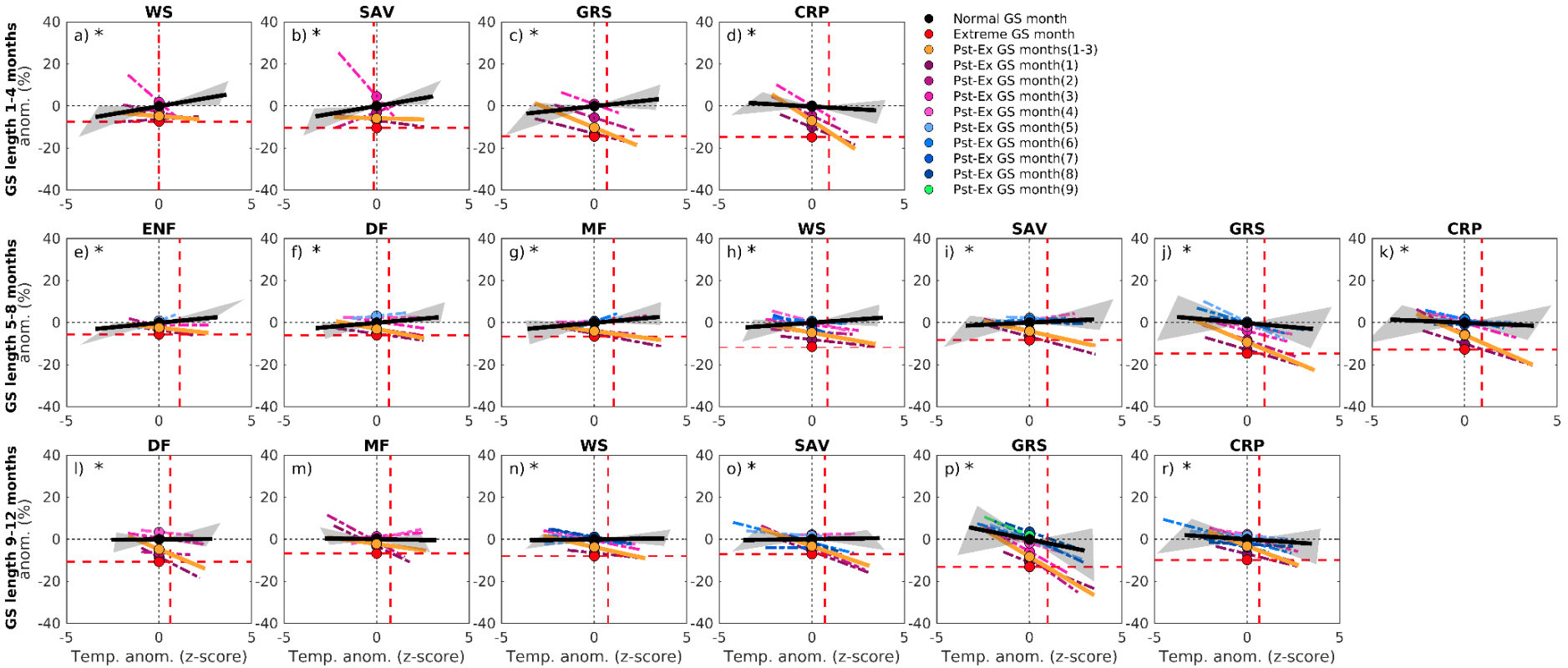

Fig. S7. Same as Fig. S5, but for EVI anomalies (y-axis, %) against the standardised 2m air temperature anomalies (x-axis, z-score).

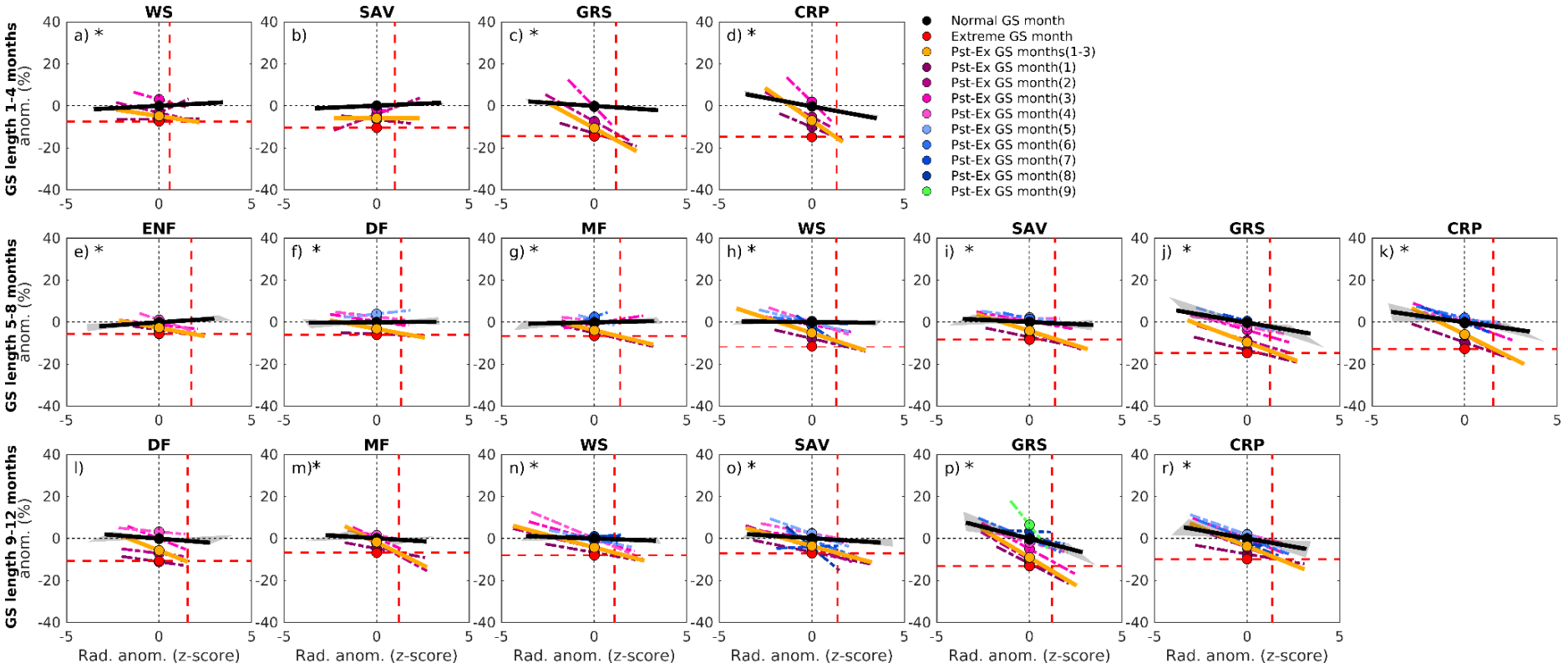

Fig. S8. Same as Fig. S5, but for EVI anomalies (y-axis, %) against the standardised surface solar radiation downwards anomalies (x-axis, z-score).

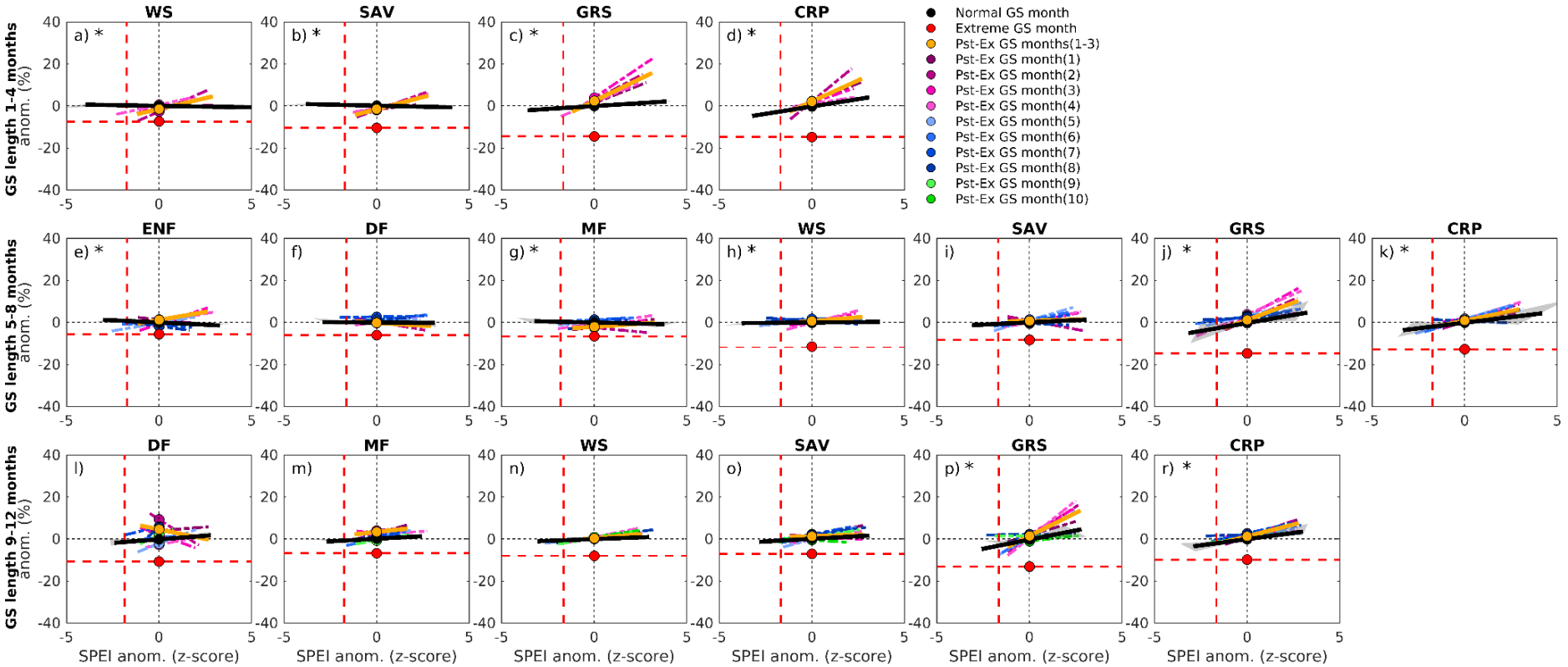

Fig. S9. Same as Fig. S5, but for the 2nd GS (i.e., next growing season after a severe drought).

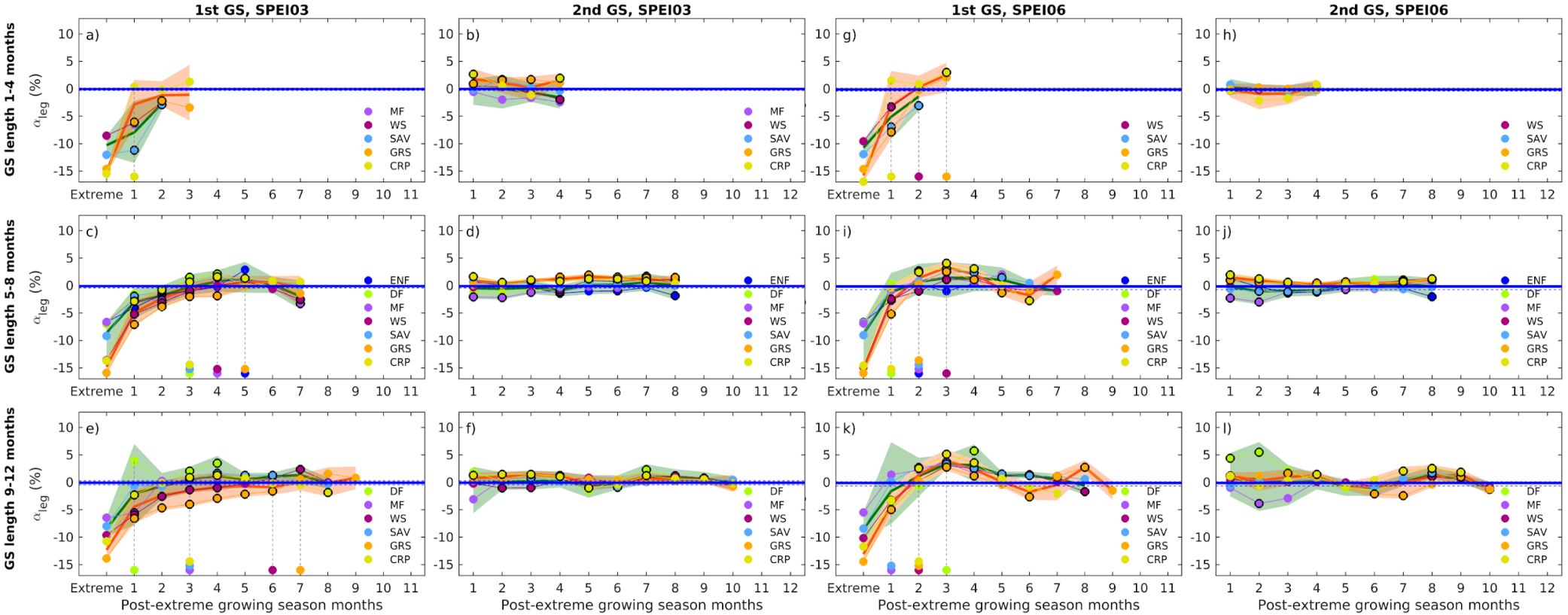

Fig. S10. Same as Fig. 2, but severe droughts are defined based on SPEI3 and SPEI6.

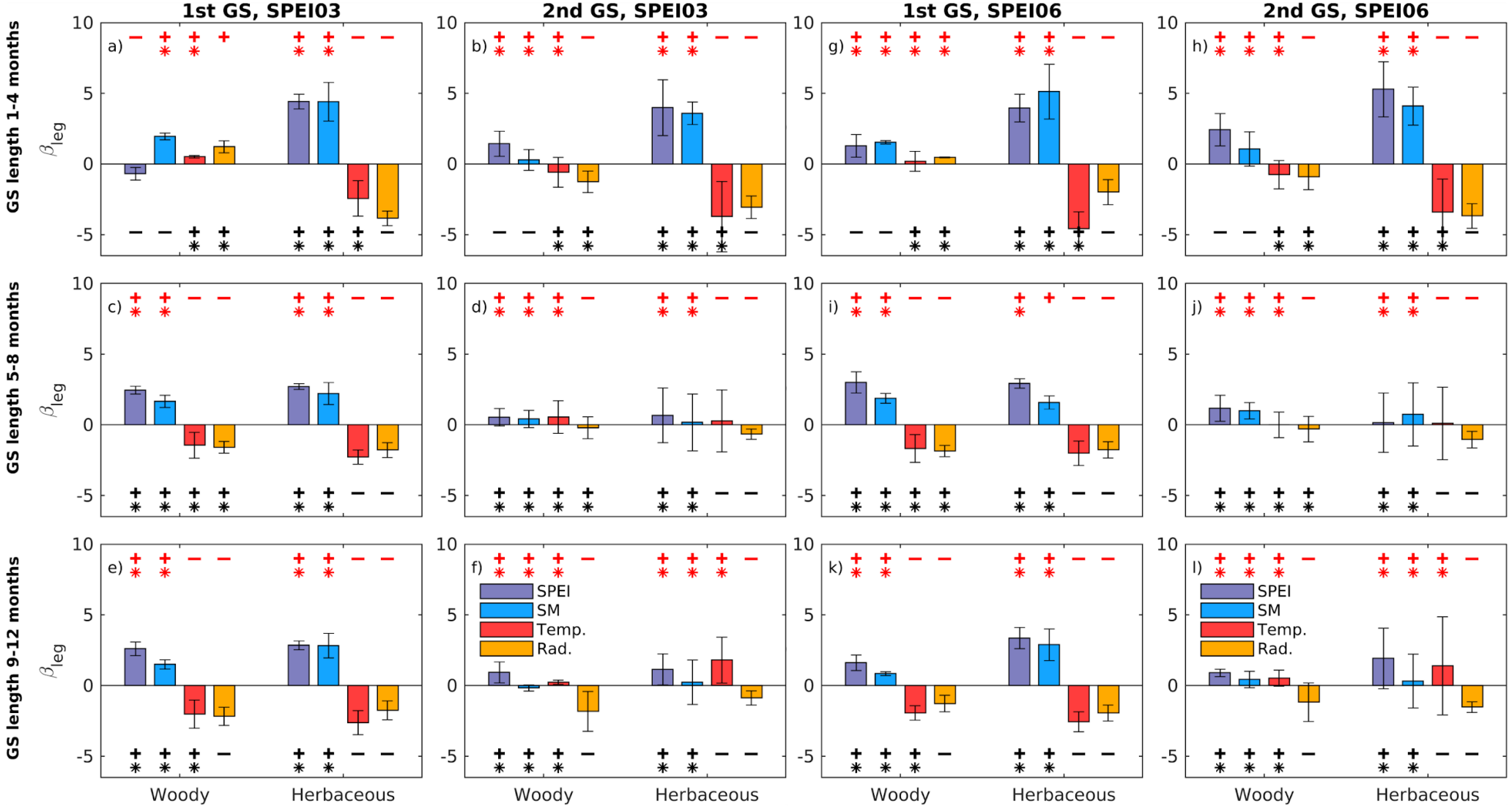

Fig. S11. Same as Fig. 3, but severe droughts are defined based on SPEI3 and SPEI6.

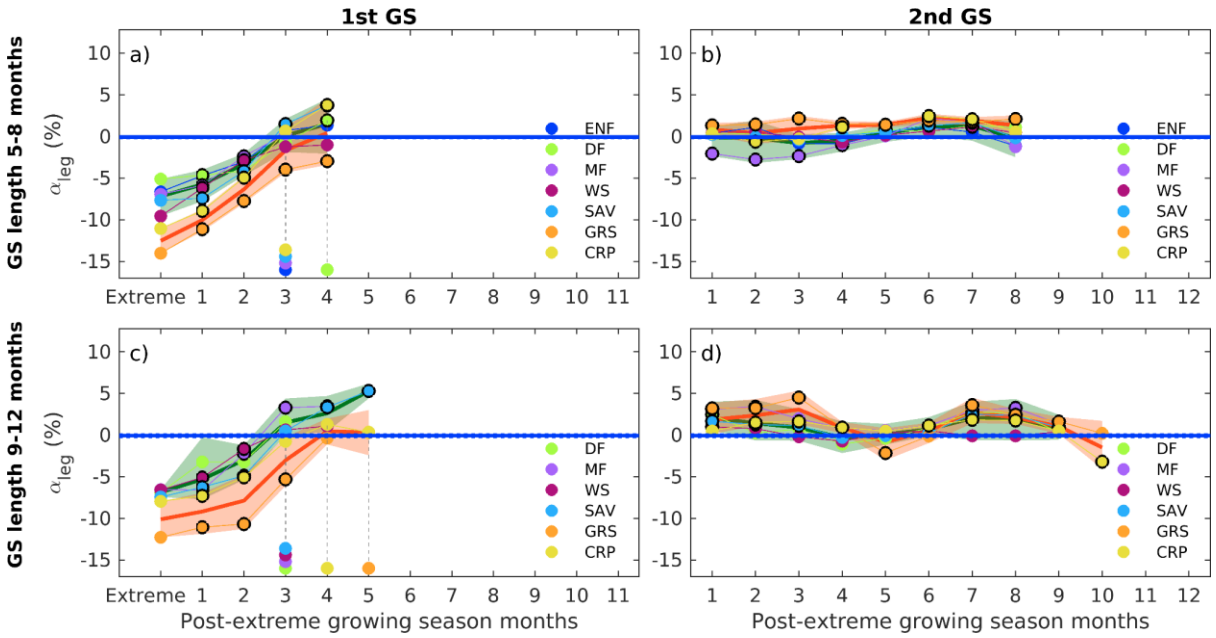

Fig. S12. Same as Fig. 2, but for the severe drought occurs during the late growing season (LGS) based on SPEI1.

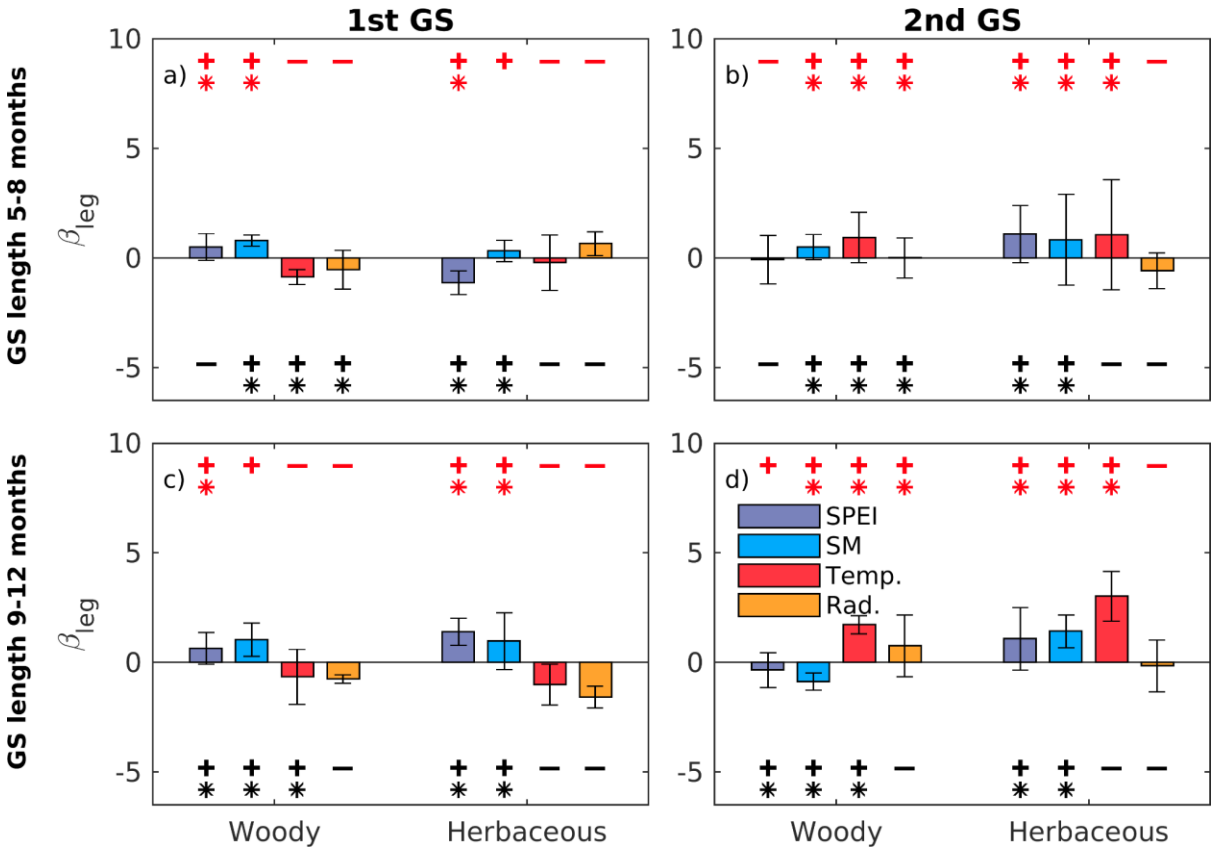

Fig. S13. Same as Fig. 3, but for the severe drought occurs during the late growing season (LGS) based on SPEI1.

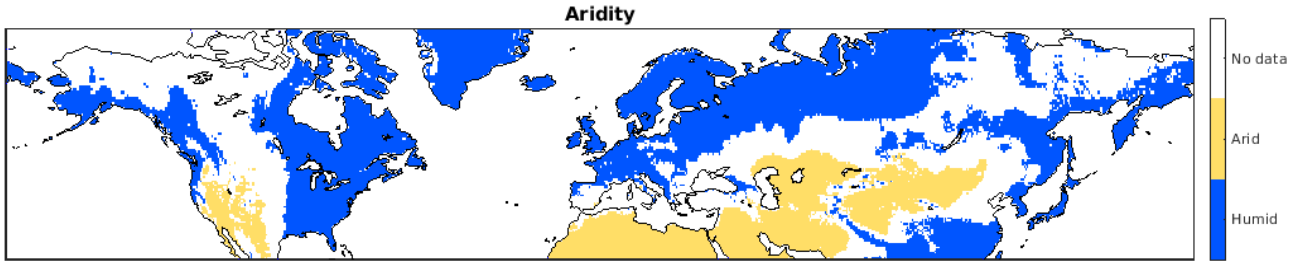

Fig. S14. Classification of aridity based on the Global Aridity Index (AI) provided by CGIAR Consortium for Spatial Information (CGIAR-CSI, see SI 1 Extended description of data). Two aridity regions are distinguished–arid regions with AI <=0.2, and humid regions with AI > 0.65.

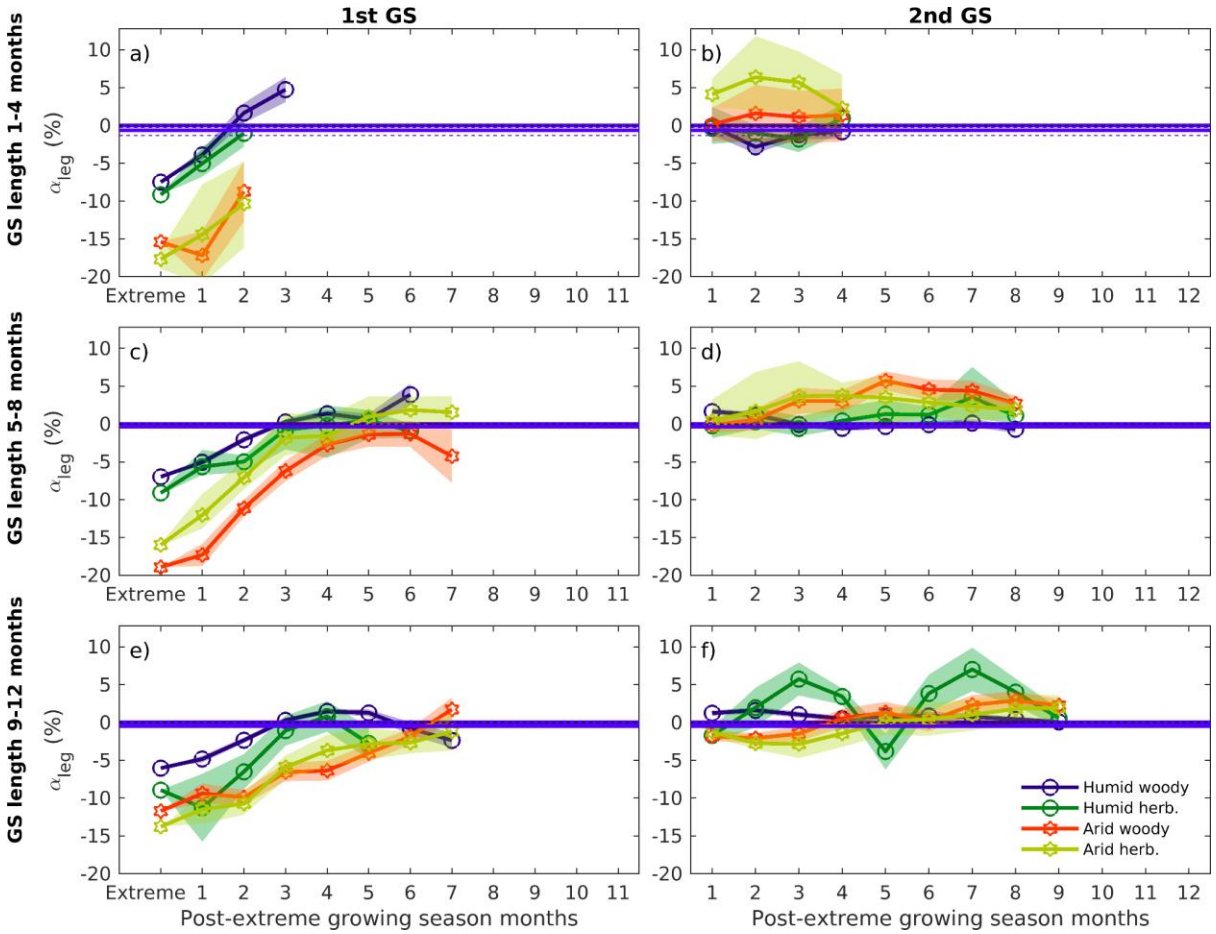

Fig. S15. Standardized changes in landclass-averaged vegetation state (α_{leg}) during the post-drought periods, as shown in Fig. 2, but based on the grouping of humid and arid regions (see Fig. S14 for the definition of humid and arid regions). Only land-cover classes that occur in both humid and arid areas are included. The woody vegetation group includes SAV and WS, and the herbaceous vegetation group includes CRP and GRS (see Fig. S3 for the definition of land-cover classes).

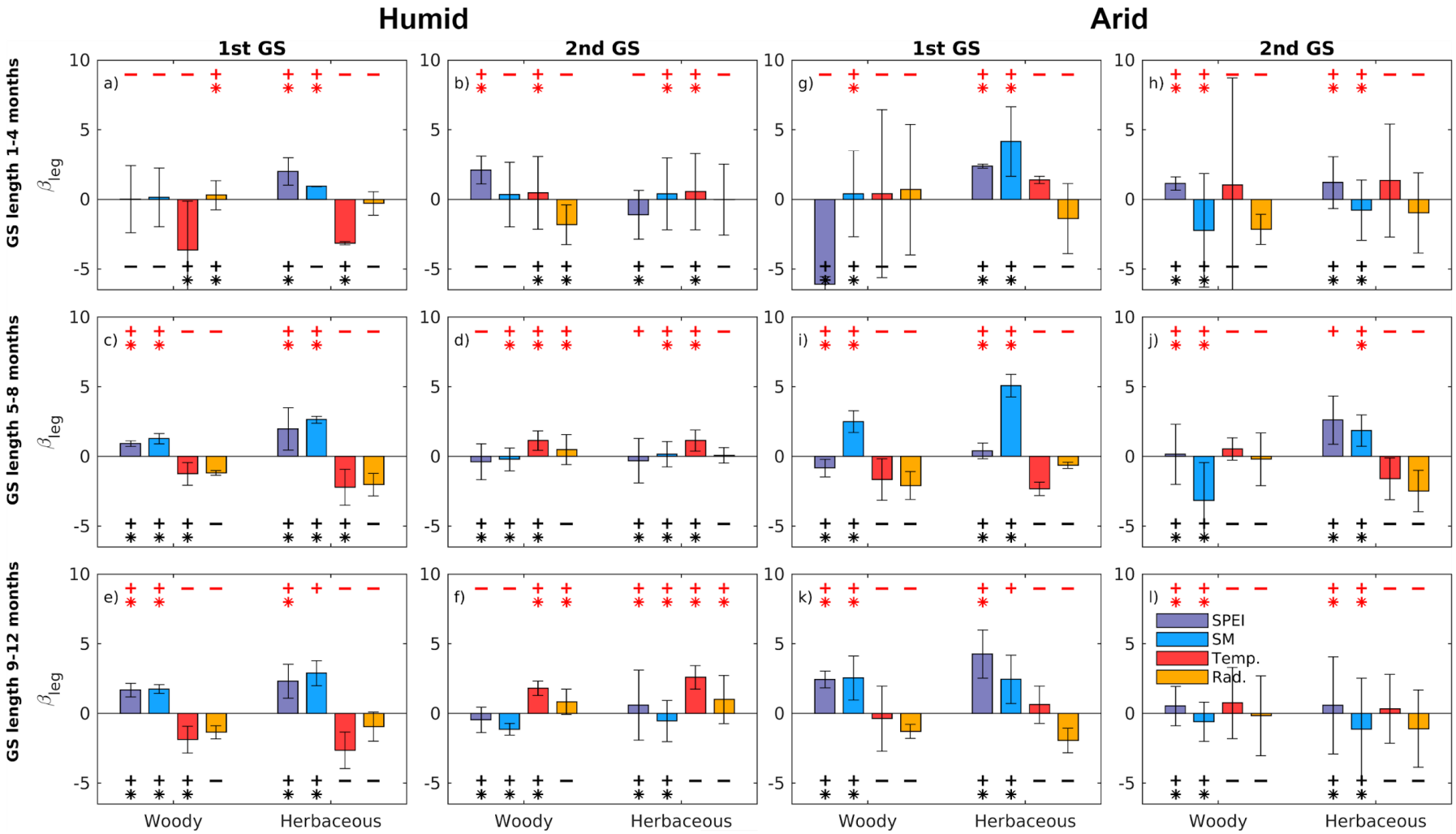

Fig. S16. Legacy effects on the sensitivity of vegetation (β_{leg}) to growing conditions (SPEI1, soil moisture, temperature and radiation), as shown in Fig. 3, but distinguishing between a)-f) humid and g)-l) arid regions. Only land-cover classes that occur in both humid and arid areas are included. The woody vegetation group includes SAV and WS, and the herbaceous vegetation group includes CRP and GRS (see Fig. S3 for the definition of land-cover classes).

References From the Supporting Information

Beck, Pan, & Miralles. (2021). Evaluation of 18 satellite-and model-based soil moisture products using in situ measurements from 826 sensors. *Hydrology and Earth System Sciences*. Retrieved from https://hess.copernicus.org/articles/25/17/2021/

Beguería, S. (2017). *sbegueria/SPEIbase: Version 2.5.1*. https://doi.org/10.5281/zenodo.834462

Friedl, M. A., McIver, D. K., Hodges, J. C. F., Zhang, X. Y., Muchoney, D., Strahler, A. H., et al. (2002). Global land cover mapping from MODIS: algorithms and early results. *Remote Sensing of Environment*, *83*(1), 287–302.

Hersbach, H., Bell, B., Berrisford, P., Hirahara, S., Horányi, A., Muñoz-Sabater, J., et al. (2020). The ERA5 global reanalysis. *Quarterly Journal of the Royal Meteorological Society*, *146*(730), 1999–2049.

Huete, A., Didan, K., Miura, T., Rodriguez, E. P., Gao, X., & Ferreira, L. G. (2002). Overview of the radiometric and biophysical performance of the MODIS vegetation indices. *Remote Sensing of Environment*, *83*(1), 195–213.

Jiao, W., Wang, L., & McCabe, M. F. (2021a). Multi-sensor remote sensing for drought characterization: current status, opportunities and a roadmap for the future. *Remote Sensing of Environment*, *256*, 112313.

Jiao, W., Wang, L., Smith, W. K., Chang, Q., Wang, H., & D'Odorico, P. (2021b). Observed increasing water constraint on vegetation growth over the last three decades. *Nature Communications*, *12*(1), 3777.

Martens, B., Miralles, D., Lievens, H., van der Schalie, R., de Jeu, R. A. M., Fernández-Prieto, D., et al. (2017). GLEAM v3 : satellite-based land evaporation and root-zone soil moisture. *GEOSCIENTIFIC MODEL DEVELOPMENT*, *10*(5), 1903–1925.

Santoro, Kirches, Wevers, & Boettcher. (2017). *Land cover CCI: Product user guide version 2.0*. ESA. Retrieved from http://maps.elie.ucl.ac.be/CCI/viewer/download/ESACCI-LC-Ph2-PUGv2_2.0.pdf

Vicente-Serrano, S. M., Beguería, S., & López-Moreno, J. I. (2010). A Multiscalar Drought Index Sensitive to Global Warming: The Standardized Precipitation Evapotranspiration Index. *Journal of Climate*, *23*(7), 1696–1718.

Wu, M., Vico, G., Manzoni, S., Cai, Z., Bassiouni, M., Tian, F., et al. (2021). Early growing season anomalies in vegetation activity determine the large-scale climate-vegetation coupling in Europe. *Journal of Geophysical Research. Biogeosciences*. https://doi.org/10.1029/2020jg006167